Available online at www.sciencedirect.com
SCIENCE DIRECT
European Journal of Mechanics A/Solids 25 (2006) 215–229

The response of clamped sandwich plates with lattice cores subjected to shock loading

G.J. McShane, D.D. Radford, V.S. Deshpande, N.A. Fleck *

Department of Engineering, University of Cambridge, Trumpington St., Cambridge, CB2 1PZ, UK

Received 3 May 2005; accepted 17 August 2005

Available online 4 October 2005

Abstract

The dynamic response of clamped circular monolithic and sandwich plates of equal areal mass and thickness has been measured by loading the plates at mid-span with metal foam projectiles. The sandwich plates comprise AISI 304 stainless steel face sheets and either AL-6XN stainless steel pyramidal core or AISI 304 stainless steel square-honeycomb lattice core. The resistance to shock loading is quantified by the permanent transverse deflection at mid-span of the plates as a function of projectile momentum. It is found that the sandwich plates have a higher shock resistance than monolithic plates of equal mass, and the square-honeycomb sandwich plates outperform the pyramidal core plates. Three-dimensional finite element simulations of the experiments are in good agreement with the experimental measurements. The finite element calculations indicate that the ratio of loading time to structural response time is approximately 0.5. Consequently, the tests do not lie in the impulsive regime, and projectile momentum alone is insufficient to quantify the level of loading.
© 2005 Published by Elsevier SAS.

Keywords: Impact loading; Sandwich plates; Lattice materials; Finite elements

1. Introduction

In a broad range of practical applications, structures are subjected to dynamic loading such that the applied loads far exceed the quasi-static collapse strength. The response of monolithic beams and plates to shock type loading has been extensively investigated. For example, Wang and Hopkins (1954) and Symmonds (1954) analysed the impulsive response of clamped circular plates and beams, respectively. Recently, Xue and Hutchinson (2003) carried out a preliminary finite element (FE) investigation of the shock response of clamped circular sandwich plates containing a foam-like core, with the effects of fluid–structure interaction neglected. Subsequently, Qiu et al. (2005) proposed an analytical model for the shock response of clamped circular sandwich plates by modifying the Fleck and Deshpande (2004) sandwich beam model. These numerical and analytical models have consistently indicated that circular sandwich plates offer a higher resistance to shock loading than monolithic plates of the same mass.

To date, there has been little experimental validation of these predictions as it is difficult to perform laboratory scale experiments with a prescribed dynamic loading history. In the recent study of Radford et al. (2005a), an experimental

* Corresponding author. Tel.: +44 1223 332650; fax: +44 1223 765046.
E-mail address: naf1@eng.cam.ac.uk (N.A. Fleck).

0997-7538/$ – see front matter © 2005 Published by Elsevier SAS.
doi:10.1016/j.euromechsol.2005.08.001

technique was developed to subject structures to high intensity pressure pulses using metal foam projectiles. The applied pressure pulses mimic shock loading in air and in water, with peak pressures on the order of 100 MPa and loading times of approximately 0.1 ms. This experimental technique has been employed by Radford et al. (2005b) and Rathbun et al. (2005) to investigate the shock resistance of clamped sandwich plates with pyramidal, square-honeycomb and corrugated lattice cores. Radford et al. (2005c) have also employed the metal foam projectiles to investigate the shock resistance of clamped circular sandwich plates with metal foam cores.

In this study we compare the shock resistance of clamped circular sandwich plates comprising stainless steel face sheets and either pyramidal or square-honeycomb lattice cores with the shock resistance of monolithic plates of equal areal mass. First, the manufacturing route of the sandwich plates is detailed and the experimental procedure described for loading the plates at mid-span by metal foam projectiles. The experimental results are compared with three-dimensional finite element predictions. These finite element calculations are used to determine the pressure versus time loading history imposed upon the monolithic and sandwich plates and thus provide information on the intrinsic dynamic strength of these plates.

2. Experimental investigation

Metal foam projectiles are used to load dynamically clamped circular sandwich plates comprising AISI 304 stainless steel face sheets with pyramidal and square-honeycomb cores, as sketched in Fig. 1. The primary objectives of the experimental investigation are:

(i) To compare the dynamic resistance of sandwich plates with monolithic plates of equal areal mass (made from the same material as the sandwich face sheets).
(ii) To investigate the effect of core topology upon the dynamic strength of the sandwich plates.
(iii) To determine the accuracy of three-dimensional finite element calculations in predicting the dynamic response of the monolithic and sandwich plates.

2.1. Specimen configuration and manufacture

Circular sandwich plates comprising pyramidal or square-honeycomb cores and AISI type 304 stainless steel face sheets were manufactured to a net areal mass m of 23.5 kg m^{-2}. The circular sandwich plates, of radius $R = 80$ mm, comprised two identical AISI 304 stainless steel face sheets of thickness $h = 1.18$ mm and density $\rho_f = 8060$ kg m^{-3}. Both the pyramidal and square-honeycomb lattice cores were manufactured with a density $\rho_c \approx 430$ kg m^{-3} and thickness $c = 10$ mm. Thus, all sandwich plates had a common final areal mass of magnitude $m = 2h\rho_f + c\rho_c \approx 23.5$ kg m^{-2}. The pyramidal lattice core comprised struts of length 17 mm and cross-section 0.9 mm × 2.0 mm as shown in Fig. 2(a). These cores were manufactured from 0.9 mm thick AL-6XN stainless steel sheets by first laser cutting square-cells to obtain a perforated sheet and then folding this perforated sheet node row

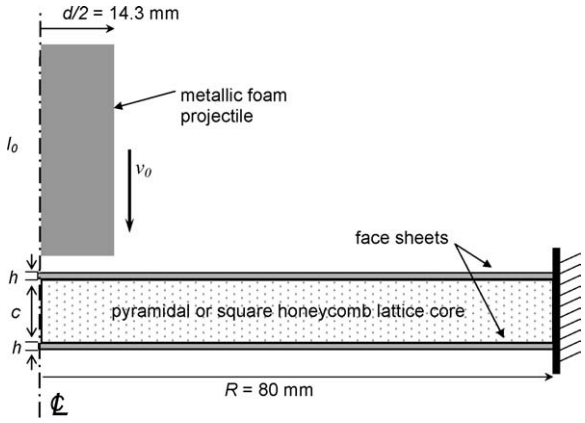

Fig. 1. Sandwich plate geometry.

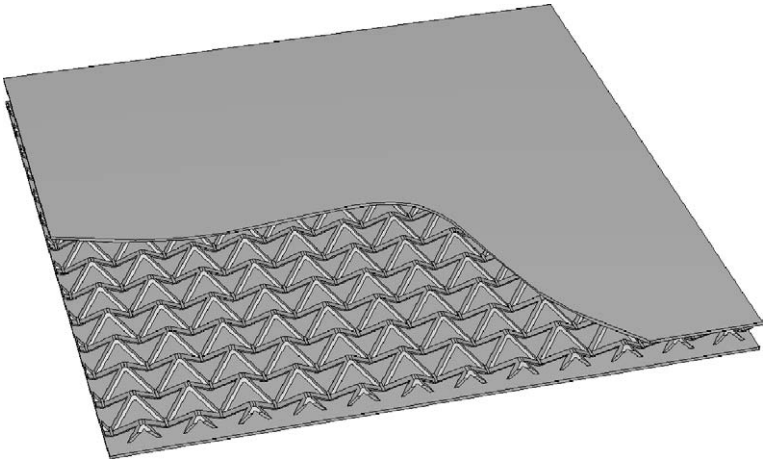

(a)

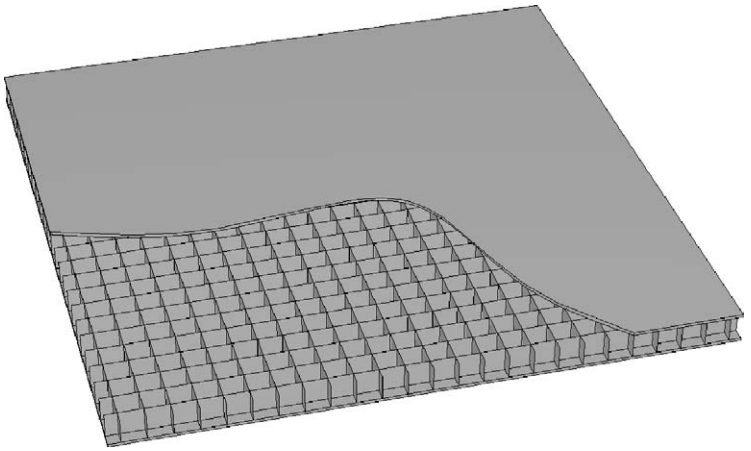

(b)

Fig. 2. Sketches of the sandwich core topologies. (a) Pyramidal core and (b) square-honeycomb core sandwich plates.

by node row to obtain regular pyramids, see Wadley et al. (2003) for details of the manufacturing route. The square-honeycomb core comprised square cells of side 10 mm, sheet thickness 0.3 mm and height $c = 10$ mm, see Fig. 2(b); this core was manufactured from 0.3 mm thick AISI 304 stainless steel sheets using the slotting technique of Cote et al. (2004).

The sandwich plate specimens were manufactured as follows. Square face sheets of dimension 250 mm × 250 mm × 1.18 mm and the pyramidal or square-honeycomb cores were clad with a thin layer of a braze powder of composition Ni–Cr 25–P10 (wt.%). Brazing was then conducted in a vacuum furnace at 1075 °C in a dry argon atmosphere at 0.03–0.1 mbar as described in Zupan et al. (2004). Eight equally spaced clearance holes for M8 bolts were drilled in these plates on a pitch circle of radius 102 mm, to enable fastening to a clamping fixture. Plan and cross-section views of the clamped plate geometry are sketched in Fig. 3. Each sandwich plate was clamped between two annular steel rings of thickness 7 mm and of inner and outer radii, 80 mm and 125 mm, respectively. The assembly was then bolted down onto a rigid loading frame by M8 bolts, as sketched in Fig. 3.

In addition to the dynamic tests on two configurations of sandwich plates, dynamic tests were also performed on AISI 304 stainless steel monolithic circular plates of areal mass $m \approx 23.5\ \mathrm{kg\,m^{-2}}$. These monolithic plates were also coated with the braze alloy and subjected to the thermal cycle used to braze the sandwich plates: this ensures that the monolithic plates have approximately the same mechanical properties as the face sheets of the sandwich plates. The monolithic plates of radius $R = 80$ mm and thickness $h = 2.92$ mm were gripped using the apparatus described above.

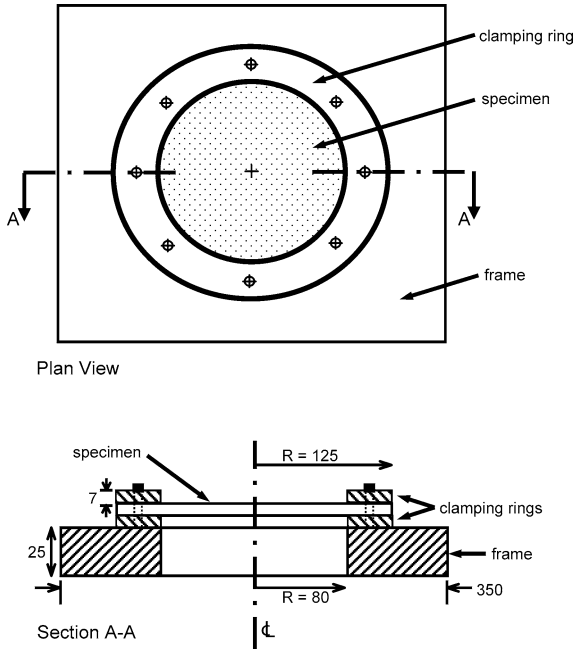

Fig. 3. Sketch of the clamping arrangement. All dimensions in mm.

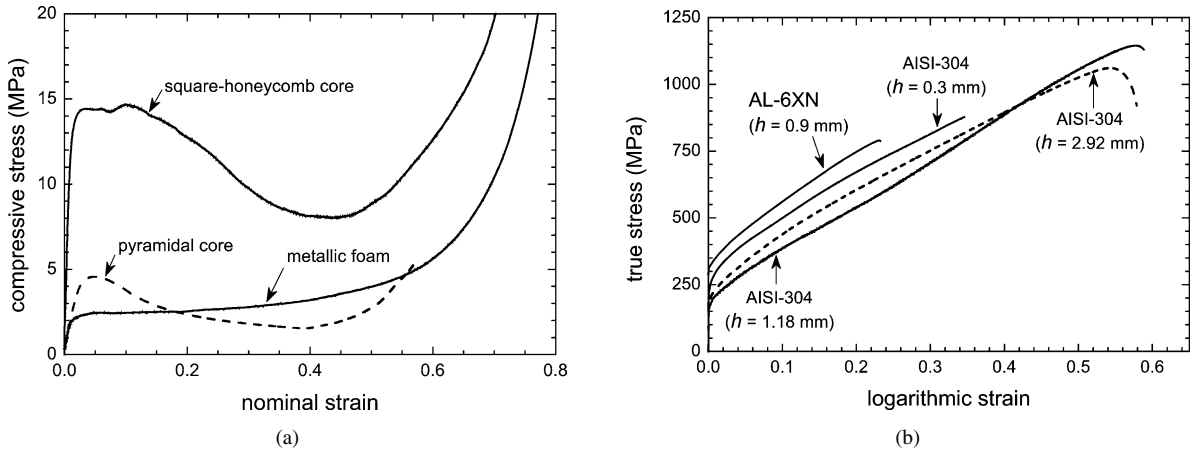

Fig. 4. (a) Quasi-static compressive response of pyramidal and square-honeycomb cores. (b) Quasi-static tensile response of the annealed AL-6XN and AISI 304 stainless steels; results are shown for the sheet thicknesses h used to manufacture the sandwich and monolithic plates.

2.2. *Properties of the constituent materials*

The uniaxial compressive responses of the pyramidal and square-honeycomb cores were measured quasi-statically at a nominal strain-rate of 10^{-3} s^{-1} using 50 mm × 50 mm sandwich plate specimens. The measured compressive nominal stress versus nominal strain responses are plotted in Fig. 4(a), and show that the pyramidal and square-honeycomb cores exhibit a peak compressive strength of approximately 5 MPa and 15 MPa, respectively, at a nominal compressive strain of approximately 5%. Both cores show a sharp increase in strength at strains exceeding approximately 0.8 and this is referred to subsequently as the densification strain ε_D. The typical uniaxial compressive response of Alporas metal foam of relative density $\bar{\rho} \approx 0.13$ is included in Fig. 4(a); this foam is used in the foam projectiles of the dynamic experiments; the measured compressive response of the foam was needed in order to determine the constitutive parameters used in the finite element simulations. The quasi-static compressive response of the foam at a strain-rate of 10^{-3} s^{-1} was measured using a cylindrical specimen similar to that of the projectile in the dynamic

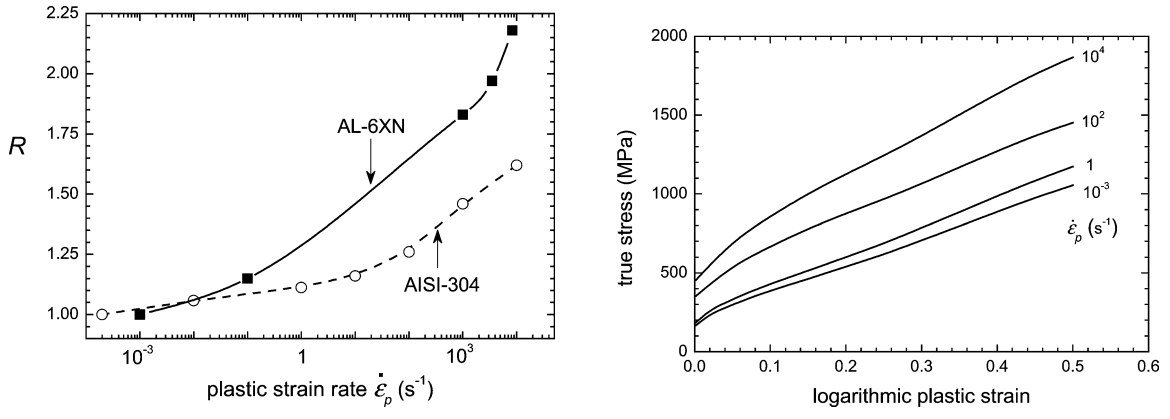

Fig. 5. (a) The dynamic strength enhancement ratio R as a function of plastic strain-rate $\dot{\varepsilon}^p$ for the AL-6XN (Stout and Follansbee, 1986) and AISI 304 stainless steels (Nemat-Nasser et al., 2001) at a plastic strain $\varepsilon^p = 0.1$. (b) Estimated tensile stress versus strain histories for the AISI 304 stainless steel ($h = 1.18$ mm) at four selected values of the applied strain-rate.

experiments (diameter 28.5 mm and length 50 mm). Unlike the lattices cores, the foam has no distinct peak strength, rather it displays plateau strength of approximately 3.5 MPa and a nominal densification strain $\varepsilon_D \approx 0.8$.

Four thicknesses of stainless steel sheet were used to manufacture the sandwich and monolithic plates. Type 304 stainless steel sheet of thickness 1.18 mm and 2.92 mm in the sandwich plate face sheets and the monolithic plates, respectively; 0.3 mm thick 304 stainless steel sheets were used in the square-honeycomb cores while the pyramidal core was manufactured from 0.9 mm thick AL-6XN sheets. Tensile specimens of dog-bone geometry were cut from each of the as-received steel sheets and then were subjected to the same brazing cycle as that used to manufacture the sandwich and monolithic plates. The uniaxial tensile responses of the four types of stainless steel sheets (in their as-brazed condition) at an applied strain-rate 10^{-3} s^{-1} are plotted in Fig. 4(b), using axes of true stress and logarithmic strain. The AISI 304 and AL-6XN stainless steels have yield strengths of approximately 200 MPa and 290 MPa, respectively. Post yield, both grades exhibit a linear hardening response with a tangent hardening modulus $E_t \approx 2.1$ GPa.

A knowledge of the high strain rate response of the 304 and AL-6XN stainless steel sheets is needed for the finite element simulations. Stout and Follansbee (1986) and Nemat-Nasser et al. (2001) have investigated the strain-rate sensitivity of the AISI 304 and AL-6XN stainless steels, respectively, for strain-rates in the range 10^{-4} s$^{-1} < \dot{\varepsilon} < 10^4$ s^{-1}. Their data are re-plotted in Fig. 5(a), where the dynamic strength enhancement ratio R is plotted against the plastic strain-rate $\dot{\varepsilon}^p$ for 10^{-3} s$^{-1} < \dot{\varepsilon}^p < 10^4$ s^{-1}. Here, R is defined as the ratio of the stress $\sigma_d(\varepsilon^p = 0.1)$ at an applied strain-rate $\dot{\varepsilon}^p$ to the stress $\sigma_0(\varepsilon^p = 0.1)$ at an applied $\dot{\varepsilon}^p = 10^{-3}$ s^{-1}. The measured stress versus strain histories presented in Stout and Follansbee (1986) and Nemat-Nasser et al. (2001) indicate that the R is reasonably independent of the choice of plastic strain ε^p at which R is calculated. Thus, the dynamic strength σ_d versus plastic strain ε^p history can be estimated as

$$\sigma_d(\varepsilon^p) = R(\dot{\varepsilon}^p)\sigma_0(\varepsilon^p), \tag{1}$$

where $R(\dot{\varepsilon}^p)$ is given in Fig. 5(a). In the dynamic finite element simulations of the experiments presented in Section 4, we employ this prescription for the strain-rate sensitivity of the stainless steels, with $\sigma_0(\varepsilon^p)$ given by the measured quasi-static stress versus strain histories for the different steels (Fig. 4(b)). As an example, the estimated true tensile stress versus logarithmic plastic strain histories of the 1.18 mm thick AISI 304 stainless steel at four selected values of applied strain-rate are sketched in Fig. 5(b).

2.3. Protocol for the dynamic tests

Alporas aluminium foam projectiles are used to provide impact loading of the clamped monolithic and sandwich plates over a central circular patch of diameter d, as shown in Fig. 1. The use of foam projectiles as a means of providing well-characterised pressure versus time has recently been developed by Radford et al. (2005a) and subse-

Table 1
Summary of the dynamic experiments performed on circular monolithic and sandwich plates. The specimens labelled M denote monolithic plates, P denotes sandwich plates with pyramidal cores, and SH denotes sandwich plates with square-honeycomb cores

Specimen	$I_0 = \rho_p l_0 v_0$ (kN s m^{-2})	ρ_p (kg m^{-3})	l_0 (mm)	v_0 (m s^{-1})	Central deflection of back face (mm)	ε_c
M1	2.00	350	52	110	0.2	–
M2	3.41	409	53	159	1.5	–
M3	5.91	378	51	307	5.8	–
M4	8.16	392	52	404	9.6	–
M5	9.54	454	48	438	12.0	–
M6	11.01	392	52	545	14.8	–
M7	12.65	451	48	585	17.7	–
P1	3.16	460	53	131	0.4	0.24
P2	6.08	377	52	313	3.8	0.60
P3	9.86	398	52	477	10.4	0.79
P4	12.30	410	52	577	14.4	0.84
SH1	3.16	439	53	137	0.3	0.01
SH2	6.05	399	49	309	4.10	0.03
SH3	9.83	447	48	458	9.55	0.37
SH4	12.11	404	52	577	11.7	0.66

quently employed to investigate the dynamic response of sandwich beams with lattice cores (Radford et al., 2005b) and circular sandwich plates with metal foam cores (Radford et al., 2005c).

Circular cylindrical projectiles of length $l_0 \approx 50$ mm and diameter $d = 28.5$ mm were electro-discharge machined from Alporas foam blocks of density ρ_p in the range 350 kg m^{-3} to 460 kg m^{-3}. The projectiles were fired from a 28.5 mm diameter bore, 4.5 m long gas gun at a velocity v_0 in the range 110 m s^{-1} to 585 m s^{-1}, providing a projectile momentum per unit area $I_0 = \rho_p l_0 v_0$ of up to approximately 13 kN s m^{-2}. Table 1 summarises the set of experiments performed, with details of the projectile density, length, impact velocity, and initial projectile momentum. The plates were examined after each experiment to measure the permanent transverse deflection of the faces, the degree of core compression and to detect any visible signs of failure.

3. Experimental results

At least four levels of initial momentum were applied to each specimen configuration by varying the density, length and impact velocity of the foam projectiles, see Table 1. The table includes the observed permanent back-face transverse deflection and level of core compression at mid-span of each specimen.

The response of the plates to shock loading is summarised in Fig. 6 as a plot of the permanent back-face deflections at mid-span versus the initial momentum of the foam projectile I_0. Both sandwich plate configurations deflect less than the monolithic plates of equal areal mass over the entire range of conditions investigated. The pyramidal and square-honeycomb core sandwich plates have similar responses up to $I_0 \approx 10$ kN s m^{-2}. Above this value of projectile momentum, the plates with a square-honeycomb core deflect less than the plates with a pyramidal core.

Define the core compressive strain as $\varepsilon_c \equiv \Delta c/c$, where Δc is the reduction in core thickness at mid-span; the dependence of ε_c upon I_0 is plotted in Fig. 7 for the two sandwich plate configurations. The strain ε_c increases with increasing I_0, but is consistently less for the sandwich plates with the square-honeycomb core. At high imposed impulses ($I_0 \geqslant 10$ kN s m^{-2}), the core compression in the pyramidal core plates is approximately constant at its densification value of 0.8.

In order to gain insight into the deformation mechanisms, the monolithic and sandwich plates tested at $I_0 \approx 13$ kN s m^{-2} were sectioned along their diametrical plane. Photographs of the diametral sections are shown in Fig. 8(a) for the monolithic plate (specimen M7, back-face deflection of 17.7 mm), in Fig. 8(b) for the sandwich plate with pyramidal core (specimen P4, back-face deflection of 14.4 mm), and in Fig. 8(c) for the sandwich plate with the square-honeycomb core (specimen SH4, back-face deflection of 11.7 mm). The diametrical profiles show that sig-

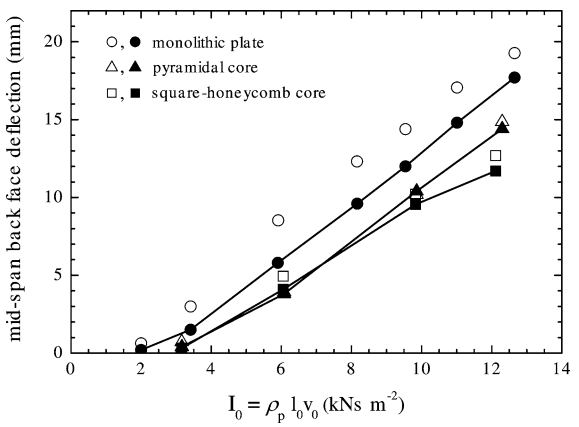

Fig. 6. Comparison of the measured and predicted permanent back-face deflection at mid-span of the dynamically loaded monolithic and sandwich plates, as a function of the foam projectile momentum I_0. Open symbols are the FE predictions and the filled symbols correspond to the experimental measurements.

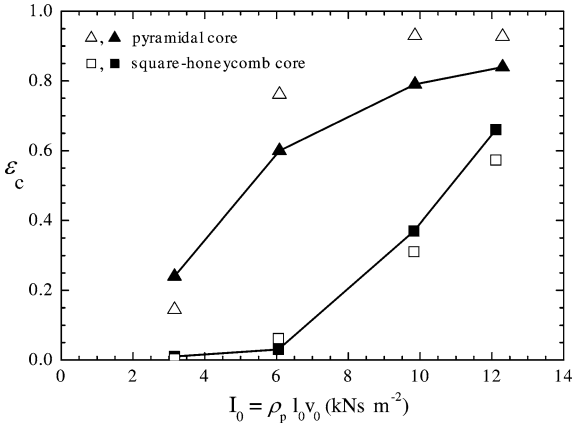

Fig. 7. Measured permanent core compression ε_c at the mid-span of the dynamically loaded sandwich plates, as a function of the initial foam projectile momentum I_0. Open symbols are the FE predictions and the filled symbols correspond to the experimental measurements.

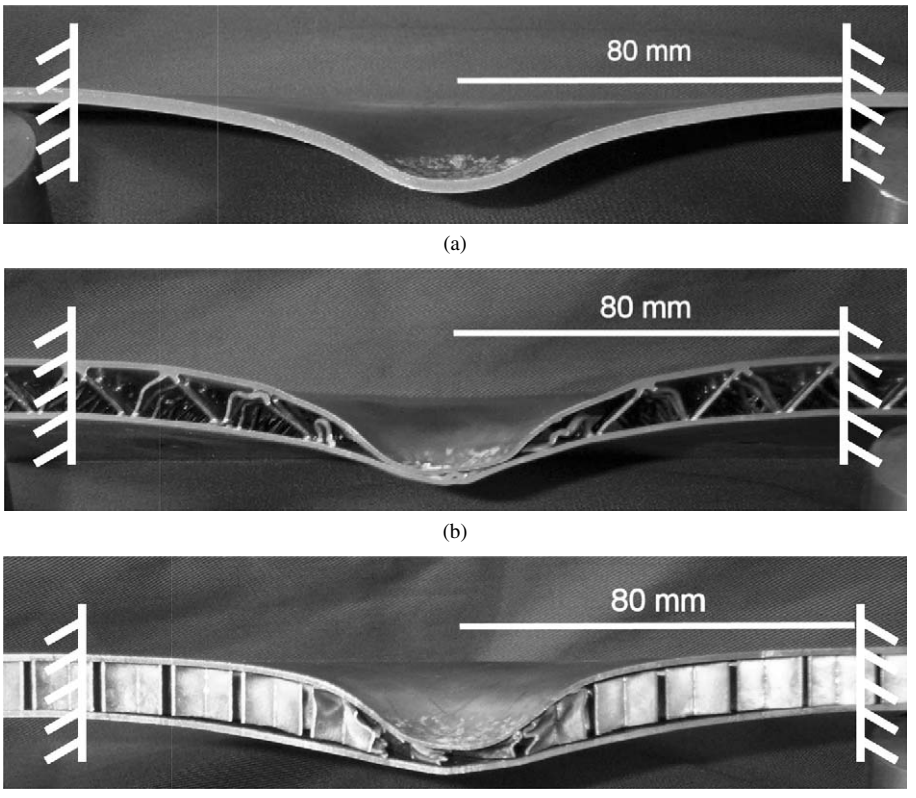

Fig. 8. Photographs of the dynamically tested specimens (a) M7, (b) P4 and (c) SHC4. All these plates were tested at $I_0 \approx 13$ kN s m^{-2} and sectioned along their diametrical plane.

nificant plastic deformation occurs in the vicinity of the foam impact and that the plates are continuously curved. It is deduced that the dynamic deformation of plates involves the formation of travelling hinges, similar to the observed behaviour of monolithic and sandwich beams reported by Radford et al. (2005b). Complete densification of

the pyramidal core occurs at the mid-span of the plate (Fig. 8(b)) while the square-honeycomb core has only partially densified. However, delamination of the square-honeycomb core from the face sheets is evident, see Fig. 8(c).

For comparison purposes, a clamped monolithic plate and the two configurations of sandwich plates have been loaded quasi-statically over a central patch. These experiments were performed at a displacement rate of 10^{-5} m s^{-1} using a flat-bottomed steel cylindrical punch of diameter 28.5 mm. The specimens were loaded until the permanent back-face deflection at the mid-span matched that obtained in the corresponding dynamic experiments with $I_0 \approx 13$ kN s m^{-2}. Subsequently, the specimens were sectioned along their diametrical planes allowing for a comparison of the dynamic and quasi-static deflection profiles. The deformed quasi-static specimens are shown in Fig. 9. It is clear that the quasi-static response is dominated by membrane action with stationary plastic hinges at the edges of the indenter and the supports (as evidenced by the discontinuity in inclination of the plates at those locations). The applied pressure (ratio of the applied load to punch cross-sectional area) versus punch displacement (front face displacement) curves obtained from the quasi-static experiments are plotted in Fig. 10. At small deflections, the strength of the plates is governed by the bending resistance of the plates and hence the sandwich plates outperform the monolithic plates. However, with increasing deflection, the membrane stretching contribution to the plate strength increases and failure modes such as face sheet delamination (Fig. 9(c)) become active in the sandwich plates. This results in monolithic plates outperforming the sandwich plates at large deflections. Similarly, we expect that these failure modes will also become active at very high impulses for the dynamically loaded plates. Such impulses were not considered in this study and hence no conclusions on the relative performance benefits of sandwich plates at high impulses can be drawn from the experiments presented here.

The core compressive strain $\varepsilon_c \equiv \Delta c/c$ in the quasi-static tests is plotted in Fig. 11 versus the back-face deflection of the sandwich plates at mid span. The core compression increases with increasing back-face deflection for the

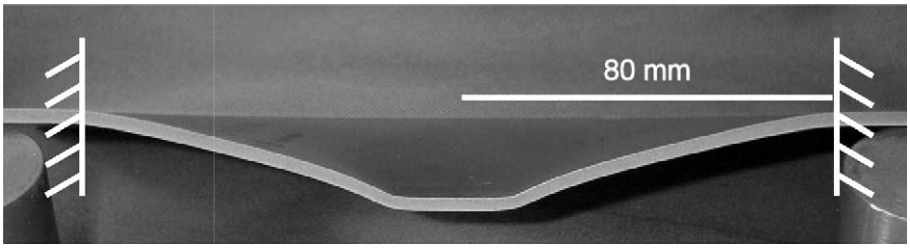

(a)

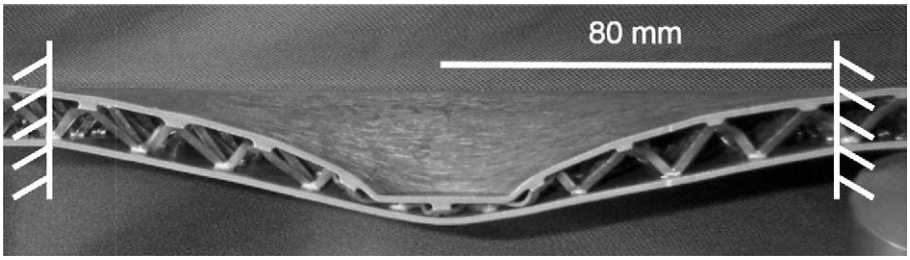

(b)

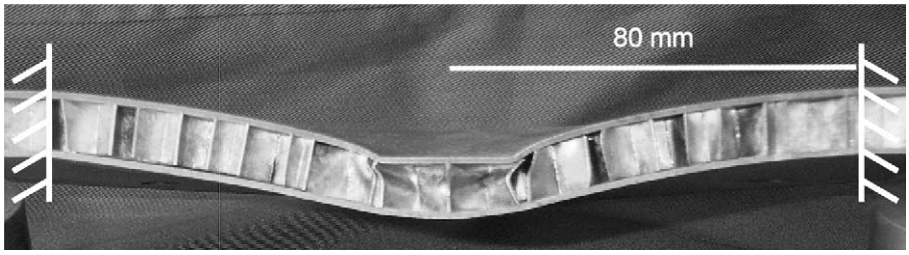

(c)

Fig. 9. Photographs of the quasi-statically tested (a) monolithic plate (b) pyramidal core sandwich plate and (c) square-honeycomb sandwich plate. These plates were loaded until the permanent back-face deflection at the mid-span matched that obtained in the corresponding dynamic experiments of Fig. 8 and sectioned along their diametrical plane.

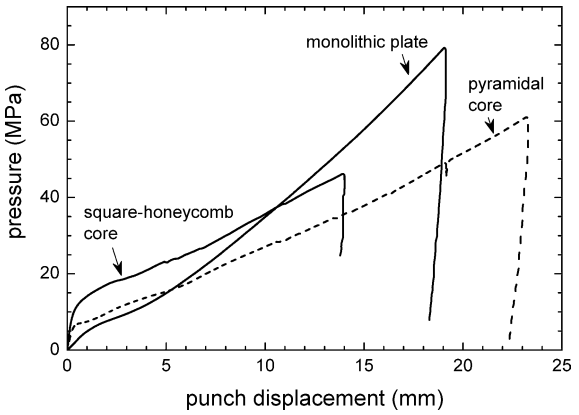

Fig. 10. Quasi-static measurements of the pressure versus punch displacements. Results are shown for the clamped monolithic plate as well as the sandwich plates with pyramidal and square-honeycomb cores.

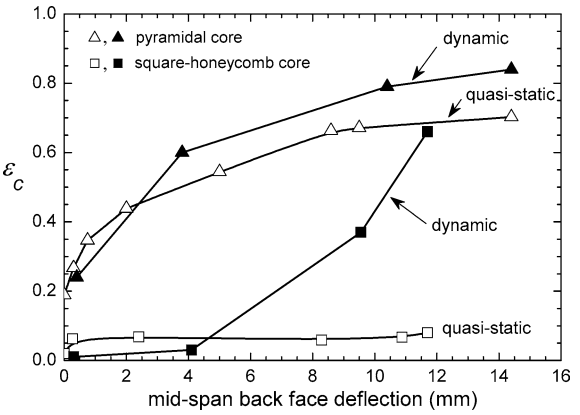

Fig. 11. Comparison between the dynamic and quasi-static measurements of the core compression ε_c as a function of the back-face deflection.

pyramidal core sandwich plates up to the densification value $\varepsilon_c = \varepsilon_D \approx 0.8$. The degree of core compression is much smaller in the square-honeycomb plates with ε_c approximately constant at 0.08. The dynamic measurements of the correlation between ε_c and back-face deflection are included in Fig. 11. A comparison of the quasi-static and dynamic measurements of ε_c indicates that while the dynamic and quasi-static core compressions are approximately equal for pyramidal core plates, the dynamic values of ε_c for the square-honeycomb plates greatly exceed the quasi-static values at the higher back face deflections.

4. Finite element simulations

Comparisons of the finite element (FE) simulations and the measured responses of the monolithic and sandwich plates are presented in this section. All computations were performed using the explicit time integration version of the commercially available finite element code ABAQUS[1] (version 6.4). Three-dimensional simulations of a quarter model of the sandwich plates and axisymmetric simulations of monolithic plates were performed. Here we briefly describe the details of these FE calculations.

Sandwich plates. Three-dimensional simulations of quarter models of the sandwich plates were performed. Along the two diametrical planes, symmetry conditions were prescribed on both the sandwich plate and the foam projectile. Clamped boundary conditions were imposed on the sandwich plates by tying the nodes on the face sheets and the core at a radius $R = 80$ mm to a rigid quarter ring. Dynamic loading of each plate was simulated by the impact of a foam projectile: at the start of the simulation, the projectile was imparted with a uniform initial velocity v_0 and was brought into contact with the plate at its mid-span. The "general contact" option in ABAQUS was employed to simulate contact between all possible surfaces including (i) the core and the face sheets, (ii) self-contact of the core, (iii) contact of the two face sheets and (iv) contact between the projectile and front face sheet. The interaction using a penalty algorithm.

The cylindrical foam projectiles of diameter 28.5 mm and length $l_0 \approx 50$ mm were modelled using linear hexahedral and wedge elements (C3D8R and C3D6, respectively in ABAQUS notation) with the elements swept about the cylindrical axis of the foam projectile. The projectiles had approximately 50 elements in the axial direction and 14 elements along the radius.

The square-honeycomb plates were modelled using four-node shell elements (S4R in ABAQUS notation) for both the face sheets and the core. Perfect bonding between the core and face sheets was assumed. All dimensions (face sheet thickness and core dimensions) were chosen to match the experimental values. An element size of 0.5 mm was employed for all the calculations reported subsequently. The pyramidal core sandwich plates were modelled using the

[1] Hibbit, Karlsson and Sorensen Inc.

four-node shell elements in the face sheets, and three-dimensional linear beam elements (B31 in ABAQUS notation) for the core struts. Again, the strut dimensions of the pyramidal core were chosen to exactly match the experimental values. The four-node shell elements in the face sheets were 0.5 mm; the pyramidal core was assumed to be perfectly bonded to the face sheets and 85 beam elements were used to discretize each strut.

Monolithic plates. The circular monolithic plates were modelled using four-node axisymmetric quadrilateral elements with reduced integration (*CAX4R* in ABAQUS notation). Clamped boundary conditions, with vanishing displacements in the radial and tangential directions, were prescribed on the outer radius of the plate, $r = R$. Dynamic loading of each plate was simulated by the impact of a foam projectile, as described subsequently. Typically, there were 160 elements along the radius of each plate and approximately three elements per millimetre through the thickness. The cylindrical foam projectiles were also modelled using *CAX4R* axisymmetric elements, with contact between the outer surface of the projectile and the top surface of the plates modelled by a frictionless contact surface as provided by ABAQUS. Similar to the 3D sandwich calculations, the projectile was discretized using 14 elements along the radius and 50 elements along it length. At the start of the simulation, the projectile was imparted with a uniform initial velocity v_0 and was brought into contact with the plate at its mid-span.

4.1. Material properties

The square-honeycomb sandwich plates and the monolithic plates were made from AISI 304 stainless steel sheets whereas the pyramidal core sandwich plates comprised a core made from AL-6XN stainless steel and face sheets made from AISI 304 stainless steel. Both grades of stainless steel were modelled as J2-flow theory rate dependent solids of density $\rho_f = 8060\ \mathrm{kg\,m^{-3}}$, Young's modulus $E = 210$ GPa and Poisson ratio $\nu = 0.3$. The uniaxial tensile true stress versus equivalent plastic strain curves at plastic strain-rates $10^{-3}\ \mathrm{s^{-1}} \leqslant \dot{\varepsilon}^p \leqslant 10^4\ \mathrm{s^{-1}}$ were tabulated in ABAQUS using the prescription described in Section 2.2 and employing the data of Fig. 5 for the AISI 304 and AL-6XN stainless steels.

The foam core and the projectile were modelled as a compressible continuum using the metal foam constitutive model of Deshpande and Fleck (2000). Write s_{ij} as the usual deviatoric stress and the von Mises effective stress as $\sigma_e \equiv \sqrt{3 s_{ij} s_{ij}/2}$. Then, the isotropic yield surface for the metal foam is specified by

$$\hat{\sigma} - Y = 0, \tag{2}$$

where the equivalent stress $\hat{\sigma}$ is a homogeneous function of σ_e and mean stress $\sigma_m \equiv \sigma_{kk}/3$ according to

$$\hat{\sigma}^2 \equiv \frac{1}{1 + (\alpha/3)^2}\left[\sigma_e^2 + \alpha^2 \sigma_m^2\right]. \tag{3}$$

The material parameter α denotes the ratio of deviatoric strength to hydrostatic strength, and the normalisation factor on the right-hand side of relation (3) is chosen such that $\hat{\sigma}$ denotes the stress in a uniaxial tension or compression test. An over-stress model is employed with the yield stress Y specified by

$$Y = \eta \dot{\hat{\varepsilon}}^p + \sigma_c, \tag{4}$$

in terms of the viscosity η is the viscosity, the plastic strain-rate $\dot{\hat{\varepsilon}}^p$ (work conjugate to $\hat{\sigma}$). $\sigma_c(\hat{\varepsilon}^p)$ is the static uniaxial stress versus plastic strain relation. Normality of plastic flow is assumed, and this implies that the "plastic Poisson's ratio" $\nu_p = -\dot{\varepsilon}^p_{22}/\dot{\varepsilon}^p_{11}$ for uniaxial compression in the 1-direction is given by

$$\nu_p = \frac{1/2 - (\alpha/3)^2}{1 + (\alpha/3)^2}. \tag{5}$$

In the simulations, the Alporas foam is assumed to have a Young's modulus $E_c = 1.0$ GPa, an elastic Poisson's ratio $\nu = 0.3$ and a plastic Poisson's ratio $\nu_p = 0$ (Ashby et al., 2000). The static yield strength σ_c versus equivalent plastic strain $\hat{\varepsilon}^p$ history is calibrated using the compressive stress versus strain response presented in Fig. 4(a). The viscosity η was set so that the shock width (Radford et al., 2005a)

$$w = \frac{\eta \varepsilon_D}{\rho \Delta v}, \tag{6}$$

has the value of $l_0/10$, where ρ is the initial foam density, ε_D the nominal densification strain of the foam, Δv the velocity jump across the shock and l_0 the initial length of the foam projectile. For the purposes of this discussion, Δv is approximately equal to the projectile velocity v_0. Thus, in these calculations $w \approx 5$ mm which is of the order observed in shock experiments (Radford et al., 2005a). Large gradients in stress and strain occur over the shock width and thus a mesh size of 1 mm was required in the foam projectile to resolve these gradients accurately.

4.2. Comparison of finite element predictions and measurements

Sample FE predictions of the mid-span deflection versus time histories of the monolithic plate specimen M9 and the pyramidal core sandwich plate specimen P4 are plotted in Fig. 12, with $I_0 = 13$ kN s m^{-2} in both cases. The figure shows the mid-span deflection of the back-face of the monolithic plate and of both front and back faces of the sandwich plate. The deflection versus time histories indicate that only small elastic vibrations occur after the peak deflection has been attained. Moreover, the peak deflection is approximately equal to the final permanent deflection for both the monolithic and sandwich plates.

The predicted mid-span, back-face deflections of the monolithic and sandwich plates are included in Fig. 6 along with the experimental measurements. The permanent deflections in the FE calculations are estimated by averaging the displacements over half a cycle of the elastic vibrations (from trough to peak) immediately after the initial peak displacement. It is concluded that the FE model predicts the permanent deflection to reasonable accuracy for the sandwich plates but slightly over-predicts the deflections of the monolithic plate. This discrepancy between the experiments and predictions for the monolithic plates might be associated with the fact that larger elastic vibrations are observed in the monolithic plates. Thus, the FE predictions plotted in Fig. 6 (which average the deflections near the initial peak deflection) might not correspond to the final permanent deflections, as measured in the experiments.

The FE predictions of the final core compression ε_c have been included in Fig. 7. The FE simulations predict the square-honeycomb measurements very well but slightly over-predict the core compression in the pyramidal core sandwich plates. This could be a result of the fact that the beam elements used to model the pyramidal core do not accurately capture the dynamic collapse modes of the pyramidal core.

The FE predictions of the deformed sandwich configurations at the point of maximum back-face deflection of the P4 and SH4 sandwich plates are shown in Figs. 13(a) and 13(b), respectively. The face sheets are plotted translucent in order to enable the deformed core to be seen. The FE predictions are in good agreement with the experimental observations of the deformed sandwich configurations (Figs. 8(b) and 8(c)).

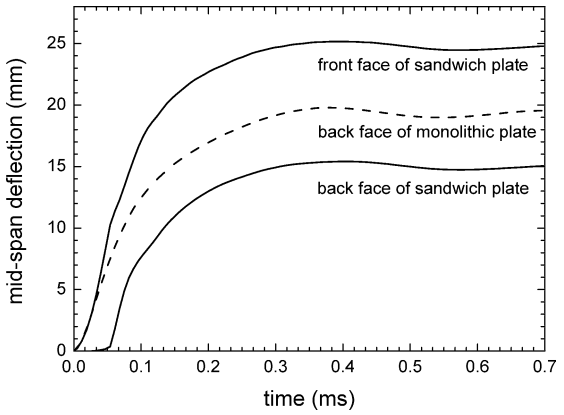

Fig. 12. Finite element predictions of the mid-span deflection versus time histories of monolithic plate specimen M7 and sandwich plate with pyramidal core (specimen P4). The figure shows the mid-span deflection of the back-face of the monolithic plate, and of both faces of the sandwich plate. $I_0 \approx 13$ kN s m^{-2}.

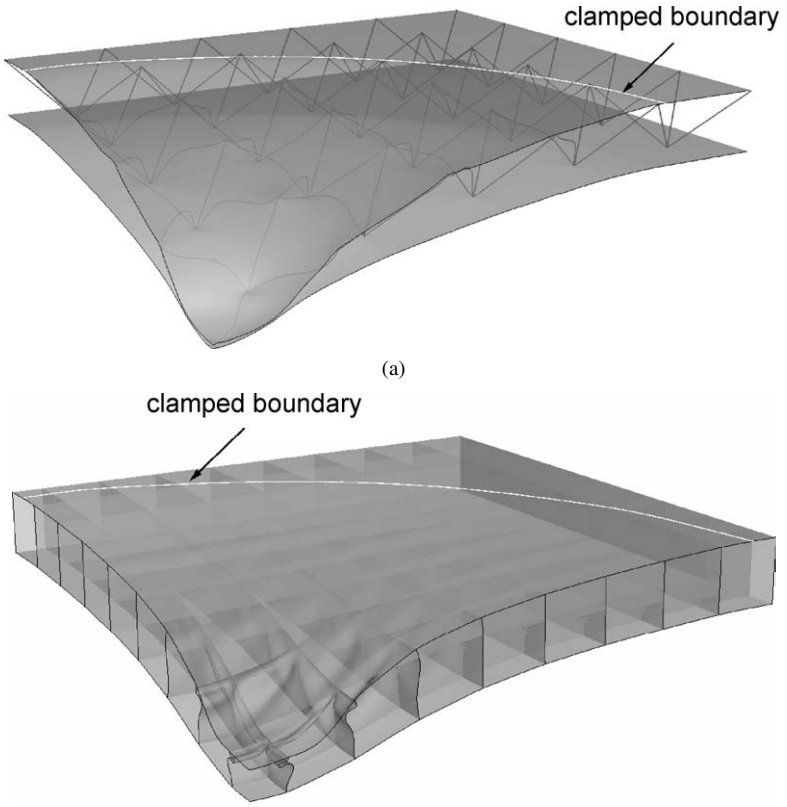

Fig. 13. Finite element predictions of the deformed sandwich configurations at the point of maximum back-face deflection for $I_0 \approx 13$ kN s m^{-2}. (a) Pyramidal and (b) square-honeycomb core sandwich plates. For the sake of clarity the projectile and rigid quarter ring not shown and the face sheets plotted translucent.

4.3. FE predictions of the pressure versus time history exerted by the foam projectiles

The pressure versus time history exerted by the foam projectile on a structure depends upon the foam projectile density ρ_p, length l_0, compressive stress versus strain response of the foam, and projectile velocity v_0. The analysis of Radford et al. (2005a) suggests that metal foam projectiles exert a rectangular pressure versus time pulse of magnitude

$$p_0 = \sigma_c + \frac{\rho_p v_0^2}{\varepsilon_D}, \tag{7}$$

and duration

$$\tau = \frac{l_0 \varepsilon_D}{v_0}, \tag{8}$$

on a rigid stationary target. Here, σ_c and ε_D are the plateau stress and nominal densification strain of the foam, respectively. This pressure versus time history, however, is sensitive to the structural response of the target: a decrease in the mechanical impedance of the target leads to a decrease in the applied pressure and to an increase in the pulse duration. Thus, it is unclear whether the observed differences in response of the various monolithic and sandwich plates for a given I_0 are due to differences in their intrinsic impact resistance, or a result of the application of different pressure time histories on the plates. We employ the FE calculations to resolve this ambiguity.

The pressure versus time history exerted by the foam projectile on the plates is derived from the FE simulations as

$$p(t) = \rho_p l_0 \dot{\bar{v}}(t), \tag{9}$$

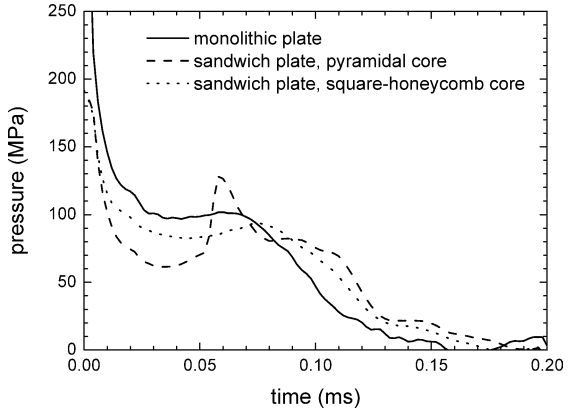

Fig. 14. The predicted pressure versus time histories exerted by the foam projectiles on monolithic specimen M7 as well as the sandwich plate specimens P4 (pyramidal core) and SH4 (square-honeycomb core). $I_0 \approx 13$ kN s m^{-2}.

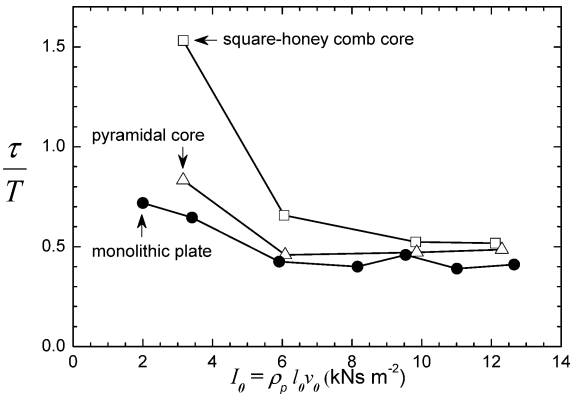

Fig. 15. FE predictions of the ratio of the loading to structural response time as a function of projectile momentum for the monolithic and sandwich plates.

where $\bar{v}(t)$ is the average axial velocity of the foam projectile at time t, and the over-dot denotes time differentiation. Momentum conservation implies that,

$$I_0 = \int_0^\infty p(t)\,\mathrm{d}t. \tag{10}$$

The calculated pressure versus time histories exerted by the foam projectiles on the monolithic plate M7, the pyramidal core plate P4 and square-honeycomb core plate SH4 are plotted in Fig. 14; in each case $I_0 = 13$ kN s m^{-2}. The differences between the pressure versus time histories are small confirming that the differences in response of the various monolithic and sandwich plates for a given I_0 are due to differences in their intrinsic impact resistance.

Consider a clamped monolithic or sandwich plate loaded with a spatially uniform pressure over a central patch of diameter d. The pressure versus time history is specified by

$$p(t) = \begin{cases} p_0, & 0 \leqslant t \leqslant \tau, \\ 0, & \text{otherwise} \end{cases} \tag{11}$$

such that the impulse is $I_0 = p_0\tau$. As discussed by Jones (1989), the loading may be considered to be dynamic if $\tau/T \ll 1$, where T is the response of the structure; in the limit $\tau/T \to 0$, the loading is impulsive. We now employ the FE calculations to determine the ratio τ/T in order to quantify the level to which the loading imposed in these foam impact experiments may be considered to be dynamic. The structural response time T is estimated from the FE calculations as the time at which the plates achieve their maximum back face deflections while the loading time τ is defined as the time at which 95% of the initial momentum of the foam projectile is transmitted into the structure, that is

$$\int_0^\tau p(t)\,\mathrm{d}t = 0.95 I_0. \tag{12}$$

The FE predictions of the ratio τ/T for the monolithic and two types of sandwich plates are plotted in Fig. 15 as a function of I_0. For $I_0 > 6$ kN s m^{-2} the ratio $\tau/T \approx 0.5$. On the other hand, for the lowest value of I_0, $\tau/T \approx 1.0$ for the monolithic and pyramidal core plates and approximately equal to 1.5 for the square-honeycomb plates. A value of τ/T greater than one implies that the pressure exerted by the foam projectile is insufficient to enable continued deformation of the plate and thus the foam projectile continues to apply pressure after the plate has arrested. It is clear that the experiments with $I_0 < 6$ kN s m^{-2} may be considered to be static for all practical purposes. Verifying this directly from the calculations and experiments presented here is difficult as the loadings applied in the dynamic and static cases are inherently different. However, the finite element calculations clearly show that the mode of deformation

at these lower impulses does not involve plastic travelling hinges and is similar to the quasi-static mode with stationary hinges at the supports and the edge of the loading patch. The experiments at the higher values of I_0 have the ratio $\tau/T < 1$ and thus dynamic by definition. It is worth noting that Jones (1989) and Xue and Hutchinson (2003) have shown that loading may be considered to be impulsive for monolithic and sandwich plates if $\tau/T < 0.01$. Thus, while I_0 has been used in this study to identify the level of loading, these experiments are not in the impulsive loading regime and I_0 alone is insufficient to define the loading.

5. Concluding remarks

Metal foam projectiles have been used to impact clamped circular monolithic plates and sandwich plates with either pyramidal or square-honeycomb lattice cores. The permanent deflections and core compression of the sandwich plates have been measured as a function of projectile momentum, and the measured responses are compared with finite element simulations. It is found that the deformation mode due to dynamic loading is different to that observed in quasi-static loading due in part to the occurrence of travelling plastic hinges in the dynamic case. Under dynamic loading the sandwich plates outperform monolithic plates of equal mass, with the square-honeycomb core plates having a higher shock resistance compared to the pyramidal core plates.

The finite element simulations capture the observed response to reasonable accuracy. These calculations also reveal that the pressure versus time histories imparted on the clamped monolithic plates are similar to those imparted on the sandwich plates for projectiles with momentum $I_0 > 6$ kN s m^{-2}. This confirms that the differences in the observed responses of the monolithic and sandwich plates for a given foam projectile momentum are due to differences in the intrinsic impact resistances of these plates. The finite element calculations predict a ratio of loading time τ to structural response time T of 0.5 in the experiments reported here. It is concluded that these experiments are not in the impulsive regime, and so the projectile momentum alone is insufficient to quantify the loading.

Acknowledgements

The authors are grateful to ONR for their financial support through US-ONR IFO grant number N00014-03-1-0283 on The Science and Design of Blast Resistant Sandwich Structures and to the Isaac Newton Trust, Trinity College Cambridge.

References

Ashby, M.F., Evans, A.G., Fleck, N.A., Gibson, L.J., Hutchinson, J.W., Wadley, H.N.G., 2000. Metal Foams: A Design Guide. Butterworth–Heinemann, Oxford.

Cote, F., Deshpande, V.S., Fleck, N.A., Evans, A.G., 2004. The out-of-plane compressive behaviour of metallic honeycombs. Mater. Sci. Engrg. A 380, 272–280.

Deshpande, V.S., Fleck, N.A., 2000. Isotropic constitutive models for metallic foams. J. Mech. Phys. Solids 48, 1253–1283.

Fleck, N.A., Deshpande, V.S., 2004. The resistance of clamped sandwich beams to shock loading. J. Appl. Mech. ASME 71 (3), 386–401.

Jones, N., 1989. Structural Impact. Cambridge University Press.

Nemat-Nasser, S., Guo, W.-G., Kihl, D.P., 2001. Thermomechanical response of AL-6XN stainless steel over a wide range of strain-rates and temperatures. J. Mech. Phys. Solids 49 (8), 1823–1846.

Qiu, X., Deshpande, V.S., Fleck, N.A., 2005. Impulsive loading of clamped monolithic and sandwich beams over a central patch. J. Mech. Phys. Solids 53 (5), 1015–1046.

Radford, D.D., Deshpande, V.S., Fleck, N.A., 2005a. The use of metal foam projectiles to simulate shock loading on a structure. Int. J. Impact Engrg. 31 (9), 1152–1171.

Radford, D.D., Fleck, N.A., Deshpande, V.S., 2005b. The response of clamped sandwich beams subjected to shock loading. Int. J. Impact Engrg., in press.

Radford, D.D., McShane, G.J., Deshpande, V.S., Fleck, N.A., 2005c. The dynamic response of clamped circular sandwich plates with metallic foam cores. Int. J. Solids Structures, in press.

Rathbun, H.J., Radford, D.D., Xue, Z., Yang, J., Deshpande, V.S., Fleck, N.A., Hutchinson, J.W., Zok, F.W., Evans, A.G., 2005. A dynamic probe for validating simulations of shock loaded metallic sandwich panels. Int. J. Solids Structures, in press.

Stout, M.G., Follansbee, P.S., 1986. Strain-rate sensitivity, strain hardening, and yield behaviour of 304L stainless steel. Trans. ASME J. Engrg. Mater. Technol. 108, 344–353.

Symmonds, P.S., 1954. Large plastic deformation of beams under blast type loading. In: Second US National Congress of Applied Mechanics.

Wadley, H.N.G., Fleck, N.A., Evans, A.G., 2003. Fabrication and structural performance of periodic cellular metal sandwich structures. Composites Sci. Technol. 63 (16), 2331–2343.

Wang, A.J., Hopkins, H.G., 1954. On the plastic deformation of built-in circular plates under impulsive load. J. Mech. Phys. Solids 3, 22–37.
Xue, Z., Hutchinson, J.W., 2003. Preliminary assessment of sandwich plates subject to blast loads. Int. J. Mech. Sci. 45, 687–705.
Zupan, M., Deshpande, V.S., Fleck, N.A., 2004. The out-of-plane compressive behaviour of woven-core sandwich plates. Eur. J. Mech. A Solids 23 (3), 411–421.